



## Numerical studies on added resistance and motions of KVLCC2 in head seas for various ship speeds

Mingyu Kim <sup>a, \*</sup>, Olgun Hizir <sup>b</sup>, Osman Turan <sup>a</sup>, Atilla Incecik <sup>a</sup>

Show more

Outline | Share | Cite

<https://doi.org/10.1016/j.oceaneng.2017.06.019>

Under a Creative Commons license

Get rights and content  
open access

### Highlights

- The optimal mesh system was investigated from the grid convergence tests for the CFD simulations.
- The added resistance and the ship motions were compared with EFD as validation study.
- The total resistance in regular waves was calculated by the CFD for three ship speeds.
- The added resistance and the ship motions were investigated with wave steepness.

### Abstract

In this study, numerical simulations for the prediction of added resistance and ship motions at various ship speeds and wave steepnesses for the KVLCC2 are presented. These are calculated using URANS CFD and 3-D potential methods, both in regular head seas. Numerical analysis is focused on the added resistance and the vertical ship motions for a wide range of wave conditions at stationary, operating and design speeds. Firstly, the characteristics of the CFD and the 3-D potential method are presented. Simulations of various wave conditions at design speed are used as a validation study, and then simulations are carried out at stationary and operating speed. Secondly, unsteady wave patterns and time history results of the added resistance and the ship motions are simulated and analysed at each ship speed using the CFD tool. Finally, the relationship between the added resistance and the vertical ship motions is studied in detail and the non-linearity of the added resistance and ship motions with the varying wave steepness are investigated. Systematic studies of the numerical computations at various ship speeds are conducted as well as the grid convergence tests, to show that the numerical results have a reasonable agreement with the available EFD results.



### Keywords

Added resistance; Ship motions; Potential flow; CFD; KVLCC2

### 1. Introduction

Now more than ever, the reduction of ship pollution and emissions, maximisation of energy efficiency, enhancement of safety requirements and minimization of operational expenditure are required and sought. Traditionally, only ship resistance and propulsion performance in calm water were considered at the ship design stage and during the design process even though recently the hull form has been optimised for a specific range of draught and speed ranges considering the operational profile (Kim and Park, 2015). However, when a ship advances in a seaway, she requires additional power in comparison with the power required in calm water due to weather effects and ship operating conditions. This degradation of the ship performance in a seaway, which is reported to be about 15–30% of the power required in calm water (Arribas, 2007) is accounted for by the application of a “Sea Margin” onto the total required engine power, and a value of 15% is typically used. The added resistance due to waves is one of the major components affecting ship performance in a seaway. Therefore, accurate prediction of the added resistance in waves is essential to evaluate the additional power requirement, to assess the full environmental impact and to design ships with high fuel efficiency in realistic operating conditions. This can also be combined with other operational measures to ensure greater efficiency, such as voyage planning and weather routing. Additionally, correct estimation and understanding of the ship motions are crucial to ensure safe navigation. Regarding international regulations, the Marine Environment Protection Committee (MEPC) of the International Maritime Organization (IMO) issued new regulations to improve the energy efficiency level of ships and to reduce carbon emissions. These regulations include the Energy Efficiency Design Index (EEDI) as a mandatory technical measure for new ships and the Energy Efficiency Operational Indicator (EEOI) which is related to ship voyage and operational efficiency as a technical measure for ships in service. Recently, the ship speed reduction coefficient ( $f_w$ ) has been proposed and is under discussion for the calculation of EEDI in representative sea states (IMO, 2012, ITTC, 2014). Moreover, guidelines for determining minimum propulsion power to maintain the manoeuvrability of a ship in adverse weather conditions (IMO, 2013) have been developed for safe manoeuvring.

The added resistance and ship motion problem in waves has been widely studied by conducting experiments and numerical simulations using potential flow theory and Computational Fluid Dynamics (CFD) approaches. There are two major analytical approaches in potential flow methods which are used to calculate the added resistance: the far-field method and the near-field method. The far-field method is based on the added resistance computed from the wave energy and the momentum flux generated by a ship and is evaluated across a vertical control surface of infinite radius surrounding the ship. This method was first introduced by Mauro (1960) using the Kochin function which consists of radiating and diffracting wave components. This method was also applied to predict the added resistance and wave drift of ships by Joosen (1966) and Newman (1967) respectively. Later on, the far-field method based on the radiated energy approach was proposed by Gerritsma and Beukelman (1972) to predict the added resistance in head seas. This approach became popular in strip theory programs due to its easy implementation. Recently, Liu et al. (2011) solved the added resistance problem with a quasi-second-order approach using the hybrid Rankine Source-Green function method considering the asymptotic and empirical methods which improved the results in short waves. Another numerical approach is the near-field method which estimates the added resistance by integrating the hydrodynamic pressure on the body surface. This method was first introduced by Havelock (1937) who used the Froude-Krylov approach to calculate hull pressures. The near-field method was enhanced by Faltinsen et al. (1980) based on the direct pressure integration approach. Salvesen et al. (1970) introduced a simplified asymptotic method based on 2-D strip theory to overcome the deficiency of this approach in short waves. Kim et al. (2007) and Joncquez (2009) formulated the added resistance based on the Rankine panel method using a time-domain approach with B-spline functions and investigated the effects of the Neumann-Kelvin (NK) and Double Body (DB) linearization schemes on the added resistance predictions. Recently, Kim et al. (2012) formulated the added resistance using a time-domain B-spline Rankine panel method based on both near-field and far-field methods in addition to the NK and DB linearization schemes for the forward speed problem. In the present study, the 3D linear potential flow method is applied to predict the ship motions and the added resistance using the NK linearization scheme and near-field method in regular waves due to more accurate prediction of ship motions and added resistance of blunt ships compared to the DB method (Kim and Shin, 2007).

Recently as computational facilities have become more powerful and more accessible, CFD tools are now commonly used to predict added resistance and ship motions. It has advantages over potential codes as it can deal directly with large amplitude ship motions and with nonlinear flow phenomena such as breaking waves and green water, without explicit approximations and empirical values. Deng et al. (2010), El Mactar et al. (2010) and Sadat-Hosseini et al. (2010) predicted the added resistance of KVLCC2 in head waves using CFD tools as presented at the Gothenburg (2010), SIMMAN (2014) and SHOPERA (2016) Workshops. Following that, Guo et al. (2012) investigated the added resistance, ship motions and wake flow of KVLCC2 in head waves with systematic validation and

verification of the numerical computation and [Sadat-Hosseini et al. \(2013\)](#) predicted the added resistance and motions for KVLCC2 using an in-house code CFDHIP-IOWA which is based on a Unsteady Reynolds-Averaged Navier-Stokes (URANS) approach. In addition to the studies on the prediction of added resistance and ship motions in waves, there have been subsequent investigations on how to reduce the added resistance by modifying the hull form. [Park et al. \(2014\)](#) and [Kim et al. \(2015\)](#) modified the fore body of KVLCC2 to reduce the added resistance in waves. Additionally, based on CFD simulations, [Kim et al. \(2014\)](#) modified the bulbous bow of a containership to optimize the hull form for both operating conditions in calm water and waves. There have also been investigations concerning the increase in the required power and the ship speed loss due to waves. [Kwon \(2008\)](#) predicted the ship speed loss using semi-empirical model considering wind, motions and diffraction resistance while [Prpić-Oršić and Faltinsen \(2012\)](#) investigated the ship speed loss and CO<sub>2</sub> emission considering added resistance due to waves and the propeller performance in actual sea, and [\(Kim et al., 2016\)](#) presented a reliable methodology to estimate the added resistance and the ship speed loss of a containership due to wind and waves in random seas.

In the study presented in this paper, the numerical simulations for the prediction of the added resistance and the ship motions for KVLCC2 in regular head waves are carried out using URANS and 3-D potential flow methods. The results obtained are validated with the available experimental data and during the study grid convergence tests are also carried out for the CFD approach. The added resistance and the vertical ship motions are examined for various wave conditions at the design and operating speeds as well as at the stationary condition. Unsteady wave patterns and the time history results of the resistance and vertical ship motions in waves are simulated using a CFD tool. The relationship between the added resistance and the ship motions for various ship speeds and wave steepness are investigated including the viscous effects and non-linear phenomena such as green water on deck.

## 2. Ship particulars and coordinate system

All calculations of the added resistance and ship motions have been performed for KVLCC2, which represents the second variant of the VLCC-type vessel developed by the Korea Research Institute of Ships and Ocean Engineering (KRISO) which is one of benchmark hull forms used to study seakeeping problems by researchers. The principal particulars of the KVLCC2 are given in full scale in [Table 1](#).

Table 1. Principal particulars of KVLCC2.

Particulars	Full scale	Model scale
Length, $L$ (m)	320	4
Breadth, $B$ (m)	58	0.725
Depth, $D$ (m)	30	0.375
Draught, $T$ (m)	20.8	0.260
Displacement, $V$ (m <sup>3</sup> )	312,622	0.6106
LCC(%), fwd +	3.48	3.48
VCG (m)	18.56	0.232
Block coefficient, $C_B$ (-)	0.8098	0.8098

For CFD simulations, a model scale vessel without appendages using a scale ratio of 1/80 is employed in the calculations.

In the numerical simulations, a right-handed coordinate system  $x, y, z$  is adopted, as shown in [Fig. 1](#).

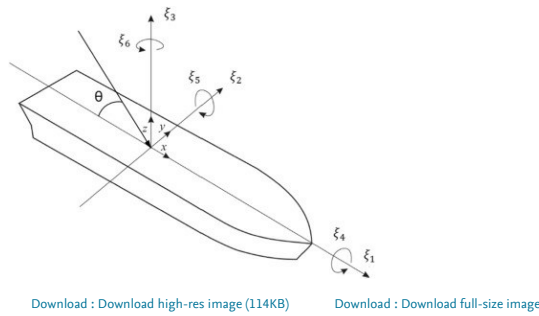


Fig. 1. Vessel coordinate system.

where the translational displacements in the  $x, y$  and  $z$  directions are  $\xi_x$  (surge),  $\xi_y$  (sway) and  $\xi_z$  (heave), and the angular displacements of rotational motion about the  $x, y$  and  $z$  axes are  $\xi_x$  (roll),  $\xi_y$  (pitch) and  $\xi_z$  (yaw) respectively and  $\theta$  angle represents the ship's heading angle with respect to the incident waves. For head seas the angle  $\theta$  equals 180° and for beam seas from the port side the angle equals 90°.

## 3. Numerical methods and modelling

In the present study, the 3-D linear potential flow and CFD methods are applied to predict the added resistance and the ship motions in regular waves.

### 3.1. 3 D linear potential method

3-D potential flow calculations are carried out using the PRECAL (PREssure CALculation) software developed by the Maritime Research Institute Netherlands (MARIN) ([Van't Veer, 2009](#)). The PRECAL software is based on the planar panel approach which can calculate the seakeeping behaviour of monohull, catamaran and trimaran ships. In addition to the rigid body motions, it can also calculate the deformation modes of a ship's hull girder, internal loads, pressure on the hull and added resistance in waves. The prediction of the forward speed effects is the main shortcoming in the solution of Green's functions due to the complex numerical integration process on the waterline sections. Numerical methods need to be implemented to solve the Boundary Value Problem (BVP) in the presence of forward speed and the Green's functions need to be satisfied both for the Free-Surface Boundary Condition (FSBC) and the Body Boundary Condition (BBC). PRECAL is a 3-D source-sink frequency domain code capable of solving the forward speed linear BVP using the Approximate Forward Speed (AFS) and the Exact Forward Speed (EFS) methods. In the AFS method the BVP is solved using zero-speed Green's functions and then forward speed corrections are applied to the BVP equations. It is possible to use the Lid panel method ([Lee and Sclavounos, 1989](#)) where waterplane area (Lid) panels are used to suppress the occurrence of the irregular frequencies in the BVP solutions. In the EFS method, exact forward speed Green's functions are used to solve the forward speed BVP, but in the PRECAL software Lid panel method can only be applied to the AFS formulation. In this study, forward speed ship motions are solved using the AFS formulation due to its fast and accurate results ([Hizir, 2015](#)). The added resistance is calculated using the near-field method based on direct pressure integration over the mean wetted hull surface, using the second-order forces to calculate wave drift forces while the first-order forces and moments are calculated to solve the ship motions. The total pressure is divided into four components which originate from the relative water height, incident wave velocities, the pressure gradient and the rotation times inertial terms. The added resistance force due to waves ( $\Delta R_{\text{wave}}$ ) is calculated in the time domain as shown in Eq. (1).

$$\Delta R_{\text{wave}} = \left[ -\rho \int_{\Omega} \frac{\partial \phi^{(1)}}{\partial t} \cdot \nabla \phi^{(1)} n^{(0)} ds \right] + \left[ -\rho \int_{\Omega} \left( \frac{\partial^2 \phi^{(1)}}{\partial t^2} \cdot \nabla \right) \left( \frac{\partial \phi^{(1)}}{\partial t} + \nabla \phi^{(1)} \cdot \nabla \phi^{(1)} \right) n^{(0)} ds \right] + \left[ \frac{1}{2} \rho g \int_{\Omega} \left( \zeta^{(0)} - \alpha^{(1)} \right)^2 n^{(0)} dt + \Omega \times M X^{(1)} \right] \quad (1)$$

where the first integral is the water velocity contribution, the second integral is the pressure gradient contribution, the third integral is the relative wave height contribution and the last term is the rotation times inertia contribution. The indices stand for the order of the forces in the force contribution formulations.  $H_0$  represents the mean position of the ship,  $a^{(1)}$  represents the first order translation and rotation vector,  $n^{(0)}$  is the zeroth order normal vector calculated on the mean position vessel wetted surface and  $a^{(1)}$  is the first order rotation vector. In order to derive the added resistance equation in the frequency domain, an oscillatory description of motion and flow is introduced and the steady flow contribution is neglected. The added resistance in the frequency domain is formulated by:

$$\Delta R_{\text{wave}} = \left[ -\rho \int_{\Omega} \left| \frac{\partial \phi^{(1)}}{\partial t} \right|^2 n^{(0)} ds \right] + \left[ -\rho \int_{\Omega} \left( \frac{\partial^2 \phi^{(1)}}{\partial t^2} \cdot \nabla \right) \left( i\omega \nabla \phi^{(1)} \right) n^{(0)} ds \right] \quad (2)$$

$$\left[ \frac{1}{2} \rho g \int_{\Omega} \left| \zeta^{(1)} \right|^2 d\Omega - \frac{1}{2} \rho g \int_{\Omega} \left| \zeta^{(2)} \right|^2 d\Omega \right] \times M X^{(1)}$$

In order to evaluate the added resistance forces, all components in the integrals are defined in perturbation series. A small parameter ( $\epsilon$ ) is introduced to represent the quantities in the perturbation series. The perturbation series expansion of the relative wave height and the velocity potential can be formulated as shown in Eqs. (3), (4):

$$\zeta = \zeta^{(0)} + \epsilon \zeta^{(1)} + \epsilon^2 \zeta^{(2)} + O(\epsilon^3) \quad (3)$$

$$\phi = \phi + \epsilon \phi^{(1)} + \epsilon^2 \phi^{(2)} + O(\epsilon^3) \quad (4)$$

where zeroth order quantities are time independent and are assumed to be small to satisfy the linearized free-surface condition. For the same reason, time-dependent parts of the series are also assumed to be small.

In added resistance calculations, only the mean values of the forces and moments are of interest. First-order quantities such as motions, velocities, accelerations etc. have a mean value of zero when the wave is given by an oscillatory function with a mean value of zero. However, second-order quantities such as added resistance have a non-zero mean value therefore in order to calculate the added resistance, second-order forces and moments need to be calculated. In the present study, in the calculation of added resistance only the constant part (mean value) of the added resistance is taken into account while the slowly oscillating part of the added resistance is trivial.

### 3.2. Computational Fluid Dynamics (CFD)

An URANS approach was applied to calculate the added resistance and ship motions in regular waves using the commercial CFD software STAR-CCM+. For incompressible flows, if there are external forces, the averaged continuity and momentum equations are given in tensor form in the cartesian coordinate system by Eq. (5) and Eq. (6).

$$\frac{\partial(\rho u_i)}{\partial t} + \frac{\partial}{\partial x_j} \left( \rho u_i u_j + \rho u_i \tau_{ij} \right) = - \frac{\partial p}{\partial x_i} + \frac{\partial \tau_{ij}}{\partial x_j} \quad (5)$$

$$\frac{\partial(\rho u_i)}{\partial t} + \frac{\partial}{\partial x_j} \left( \rho u_i u_j + \rho u_i \tau_{ij} \right) = - \frac{\partial p}{\partial x_i} + \frac{\partial \tau_{ij}}{\partial x_j} \quad (6)$$

where  $u_i$  is the relative averaged velocity vector of flow between the fluid and the control volume,  $\tau_{ij}$  is the Reynolds stresses and  $p$  is the mean pressure. For Newtonian fluid under incompressible flow, the mean shear stress tensor,  $\tau_{ij}$ , is expressed as Eq. (7).

$$\tau_{ij} = \mu \left( \frac{\partial u_i}{\partial x_j} + \frac{\partial u_j}{\partial x_i} \right) \quad (7)$$

where  $\mu$  is dynamic viscosity.

The finite volume method (FVM) and the volume of fluid (VOF) method were applied to the spatial discretization and free surface capturing respectively. The flow equations were solved in a segregated manner using a predictor-corrector approach. Convection and diffusion terms in the RANS equations were discretized by a second-order upwind scheme and a central difference scheme. The semi-implicit method for pressure-linked equations (SIMPLE) algorithm was used to resolve the pressure-velocity coupling and a standard  $k-\epsilon$  model was applied as the turbulence model. In order to consider ship motions, a Dynamic Fluid Body Interaction (DFBI) scheme was applied with the vessel free to move in heave and pitch directions as vertical motions.

Only half of the ship's hull (the port side) with a scale ratio of 1/80 and control volume were taken into account in the calculations; thus, a symmetry plane formed the centreline domain face in order to reduce computational time and complexity. The calculation domain is  $-3L < x < 1.25L$ ,  $0 < y < 2L$ ,  $-2L < z < 1L$  where the mid-plane of the ship is located at  $y = 0$  and ship draught (T) is at  $z = 0$ . The boundary conditions together with the generated meshes are depicted in Fig. 2. Artificial wave damping was applied to avoid the undesirable effect of the reflected waves from the side and outlet boundaries.

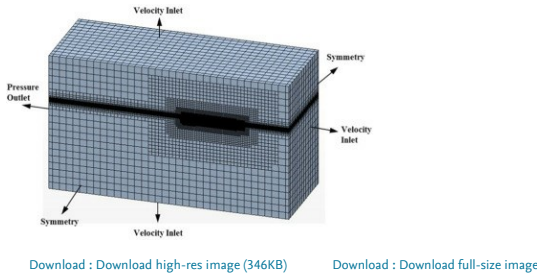


Fig. 2. Mesh and boundary conditions.

## 4. Discussion of results

In this section, the simulation results using CFD and 3-D potential methods are presented and compared with available experimental added resistance (Lee et al., 2013) and ship motions data in regular head waves. Unsteady wave patterns and time history results of the resistance and vertical ship motions in waves are simulated using a CFD method. Only two degrees of freedom motions, which are heave and pitch responses, are calculated during all simulations.

### 4.1. Grid convergence test

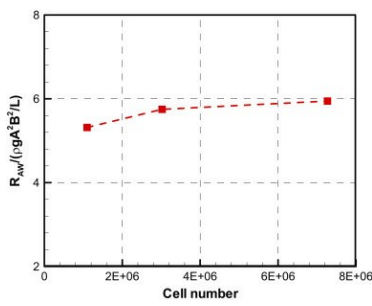
Prior to the investigation of the added resistance and the heave and pitch motions using the CFD tool, grid convergence tests are performed to capture the accurate wavelength and height on the free surface. The CFD simulations at 15.5 knots, which corresponds to the Froude Number (Fn) of 0.142, are carried out and the simulation results are compared with the available experimental data. Grid convergence tests are performed at the wavelength to ship length ratio ( $\lambda/L$ ) of 1.2 and at the wave steepness ( $H/\lambda$ ) 1/60. This wave condition corresponds to a resonant case (Sadat-Hosseini et al., 2013). The coarse and fine mesh systems are derived by reducing and increasing cell numbers per wavelength and cell height on free surface respectively using a factor of  $\sqrt{2}$  (Böckmann et al., 2014) as well as cell numbers on and around the ship hull, which is affected by the mesh refinement on free surface, based on the base mesh case (Grid no G2, Case no. C10). The simulation time step is set to be proportional to the grid size as shown in Table 2.

Table 2. Test cases for grid convergence ( $\lambda/L = 1.2$ ,  $H/\lambda = 1/60$ ,  $V_s = 15.5$  knots).

Grid name	Case no.	Mesh	$\lambda/\Delta x$	$H/\Delta z$	$T_e/\Delta t$
G <sub>1</sub>	C1F	Fine	140	28	362
G <sub>2</sub>	C10	Base	100	20	256 (2 <sup>8</sup> )
G <sub>3</sub>	C1C	Coarse	70	14	181

where  $T_e$  represents the corresponding encountering period.

The results of the convergence tests with three different mesh systems are shown in Fig. 3 where  $\rho$ ,  $g$  and  $A$  denote the density, gravitational acceleration and the wave amplitude parameters respectively. As the number of cells increased, the added resistance coefficient increased, especially from the coarse mesh (G<sub>3</sub>) to base mesh system (G<sub>2</sub>).



Download : [Download high-res image \(129KB\)](#) Download : [Download full-size image](#)

Fig. 3. Grid convergence test for the added resistance ( $V_s = 15.5$  knots,  $\lambda/L = 1.2$ ,  $H/\lambda = 1/60$ , model scale).

Additionally, in the current study, the grid uncertainty analysis is conducted using grid triplets  $G_1$ ,  $G_2$  and  $G_3$  with a uniform parameter ratio ( $r_G$ ) chosen to be  $\sqrt[3]{7}$  for the free surface refinement.  $S_1$ ,  $S_2$  and  $S_3$  are the corresponding solutions of the added resistance using the fine, base and coarse grids respectively and  $R_k$  is the convergence ratio as given in Eq. (8).

$$R_k = \frac{\epsilon_{k+1}}{\epsilon_{k+2}} \quad (8)$$

where  $\epsilon_{k+1} = S_{k+1} - S_k$  and  $\epsilon_{k+2} = S_{k+2} - S_{k+1}$  are the differences between base-fine and coarse-base solutions and subscript  $k$  refers to the  $k$ th input parameter which is  $G$  (i.e. grid-size) in this study. Grid uncertainty study shows a monotonic convergence for the added resistance with  $R_k = 0.478$  and the grid uncertainty with  $\epsilon_G = 3.759\% S_1$  based on the Grid Convergence Index (GCI) method. Results reveals that the effects of the grid changes are small for the present range of grid size (Sadat-Hosseini et al., 2010). For more detailed information on the calculation of the uncertainty analysis, reference can be made to Stern et al. (2006). Therefore the base mesh system was chosen for the CFD simulations in this study while the cell number and time step vary according to the wave conditions in the simulations.

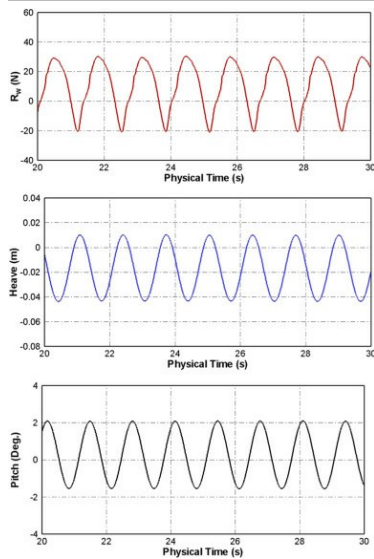
In the 3-D potential flow method calculations, half of the ship's hull under the still water level is modelled using around 1800 quadratic and triangular panels while 8 panels per wavelength as the maximum length of each panel are used for the highest encounter frequency. Regarding the computational time, for 3-D potential flow method the computational cost for each wave frequency, wave direction and ship speed is about 20 s (single CPU at 2.7 GHz). The CFD method costs about 1.5–2 days (36 CPUs at 2 GHz) for one wave condition, which means that the 3-D potential method is much more cost efficient than the CFD for the calculations of the added resistance and ship motions. However, in 3-D potential method viscosity cannot be implemented in the calculations due to the rigid-body linear method ship motions and added resistance might be over-estimated around the resonant frequencies.

The added resistance due to waves ( $R_{sw}$ ) is obtained by Eq. (9).

$$R_{sw} = R_w - R_c \quad (9)$$

where  $R_w$  and  $R_c$  are total resistance in waves and resistance in calm water respectively.

Fig. 4 shows the results of the time history for the ship total resistance, the heave and the pitch motions in waves which are oscillating periodically with a corresponding encounter period ( $T_e = 1.3227$  s) as shown in Table 3.



Download : [Download high-res image \(398KB\)](#) Download : [Download full-size image](#)

Fig. 4. Time histories of total resistance, heave and pitch motions in waves (Case: C10, model scale).

Table 3. Test cases at design speed (15.5 knots).

Case no.	$V_s$ [knots]	Wavelength ( $\lambda/L$ )	Wave height ( $H$ ) [m]	Wave steepness ( $H/\lambda$ )	$f_e$ [Hz] (model)	$T_e$ [sec.] (model)
C00	15.5	Calm water	–	–	–	–
C10		1.20	6.40	1/60	0.7560	1.3227
C11		0.50	2.67		1.3293	0.7523
C12		0.75	4.00		1.0186	0.9818
C13		1.00	5.33		0.8476	1.1798
C14		1.40	6.40		0.6872	1.4552
C15		1.60	7.47		0.6332	1.5793

#### 4.2. Added resistance and ship motions at design speed

Following the CFD grid convergence tests, numerical calculations using the 3-D potential and CFD methods at the design speed of 15.5 knots were carried out in both calm water and wave conditions

for various wavelengths for constant wave steepness ( $H/\lambda$ ) of 1/60. The test cases are summarised in Table 3.

The wavelength is assumed to be  $\lambda = gT^2/2\pi$  for deep water and the wave encountering frequency  $f_e$  in Hz for model scale is calculated by  $f_e = \sqrt{g/(2\pi\lambda)} + U/\lambda$  for head sea where  $U$  denotes the ship forward speed in m/s.

Prior to the investigation of the added resistance, **Response Amplitude Operators** (RAOs) of heave and pitch motions are compared with the available experimental data (Larsson et al., 2010) and numerical results (Seo et al., 2014) as shown in Fig. 5. It is a well-known fact that the added resistance increases with the relative motions, hence heave and pitch motions, and inaccuracies in the predicted motion responses may amplify the errors in the added resistance calculations. In this study,  $\xi_z$  and  $\xi_\theta$  are the amplitudes of heave and pitch motion responses respectively whereas  $k = 2\pi/\lambda$  is the wave number in deep water. The motion responses are evaluated at the ship's **centre of gravity**. The zeroth and first order terms of the resistance and motion responses calculated by CFD are used for the added resistance coefficient and motion transfer functions (Shen and Wan, 2013). The overestimation of the heave motion using the 3-D potential method is amplified around the resonance period ( $1.0 < \lambda/L < 1.4$ ), while CFD method slightly underestimates the heave motion around the resonance period for the range of  $\lambda/L$  from 1 to 1.4. For the pitch motions, the results obtained from both methods show good agreement with the experimental data. The overestimation of the results obtained from the 3-D potential method for the heave motions can be attributed to the AFS formulation, in which the BVP is solved using zero speed **Green's functions** and then forward speed corrections are applied to the boundary conditions, and also to the Neumann-Kelvin (NK) approximation where the steady wave and unsteady wave interactions are linearized. Kim and Shin (2007) presented a study about the steady and **unsteady flow** interaction effects on advancing ships and showed that in heave and pitch responses the NK approach overestimates the heave and pitch responses compared to the experimental results, whereas the Double-Body (DB) and Steady Flow approaches agreed well with the experiments. The underestimation of the results obtained from the CFD method is likely to stem from the adoption of a non-inertial reference frame in which large amplitude motion causes inaccurate capturing of the free surface.

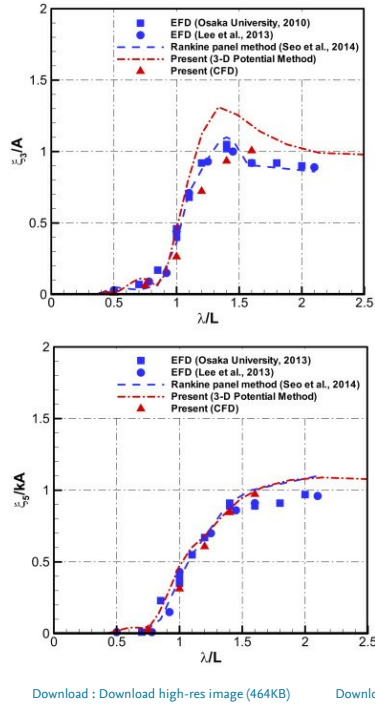


Fig. 5. Heave and pitch responses ( $V_s = 15.5$  knots,  $\theta = 180^\circ$ ).

The numerical results of the added resistance are compared with the available experiment data (Lee et al., 2013) and numerical results (Seo et al., 2014) as illustrated in Fig. 6, which indicates that the CFD and 3-D panel methods both have a reasonable agreement with the experimental data except around the resonance period where both methods underestimate the added resistance. The authors will address this problem in future studies using a developed 3-D potential method and adaptive mesh method in CFD simulations.

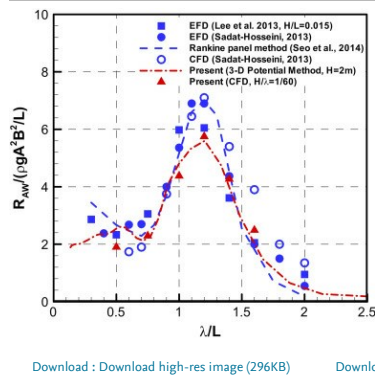
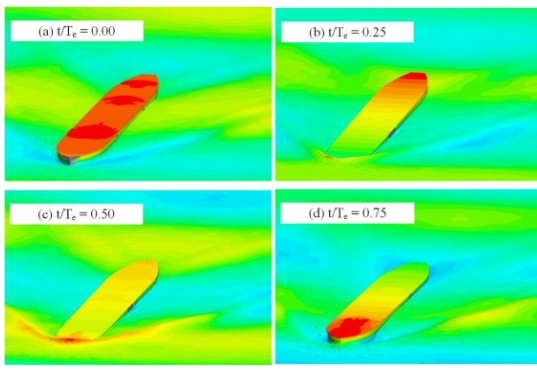


Fig. 6. Added resistance ( $V_s = 15.5$  knots,  $\theta = 180^\circ$ ).

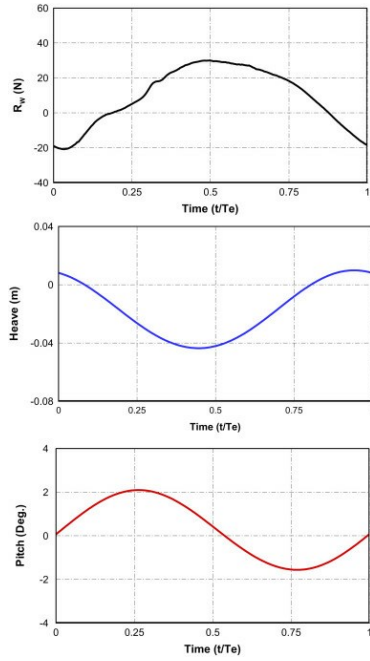
To visualise the ship motions and periodic wave patterns, the C10 test case is selected in which the maximum added resistance is recorded. Four snapshots of the waves and the vessel motions were captured with respect to the period of encounter at  $\lambda/L = 1.2$  and at a vessel speed of 15.5 knots. Results displayed in Fig. 7 show that the phenomenon of water on deck has been successfully captured by the current CFD model. Fig. 7(c) is the snapshot at  $t/T_e = 0.5$  when the ship has the largest resistance value as is shown in Fig. 8. In Fig. 7 the contour on the **hull and free surface** indicates water height level taking into account the ship vertical motions. Similarly to the snapshots in Fig. 7, the time histories of total resistance force, heave and pitch motions are displayed over an encounter period as shown in Fig. 8. The largest resistance force in waves is observed around  $t/T_e = 0.5$  when the bow is completely immersed and when the relative wave height is high around the bow with green water on deck, as illustrated in Fig. 7(c). The position of the vessel where the maximum resistance is recorded is when the ship has the highest immersion due to heave motion, while the pitch amplitude is almost zero.



Download : [Download high-res image \(591KB\)](#)

Download : [Download full-size image](#)

Fig. 7. Snapshots of free surface elevation over one period of encounter (Case no. C10,  $V_s = 15.5$  knots,  $\lambda/L = 1.2$ ).



Download : [Download high-res image \(359KB\)](#)

Download : [Download full-size image](#)

Fig. 8. Total resistance, heave and pitch response time histories at a period of encounter (Case no. C10, model scale).

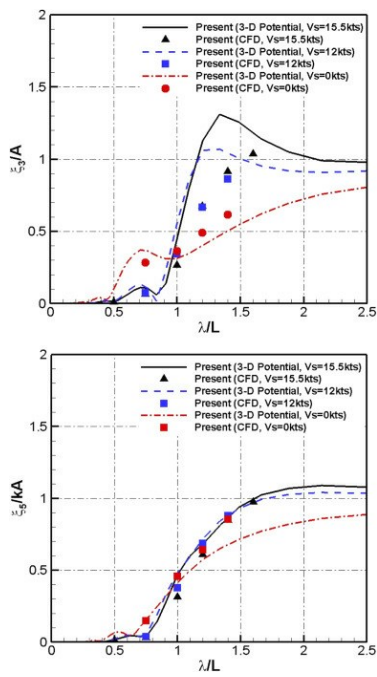
#### 4.3. Added resistance and ship motions at stationary condition and at operating speed

To consider the slow steaming or the realistic operating speeds of the vessel, the effect of ship speed on the added resistance and ship motions was investigated (Tezdogan et al., 2015). In addition to the assumed operating speed (12 knots) as it was applied in SHOPERA (2016) Workshop, the cases for the stationary condition (0 knots) were also simulated as summarised in Table 4. Wave conditions for wavelength and height are considered identical to those considered in the simulations with the design speed cases.

Table 4. Test cases at operating speed (12 knots) and at stationary conditions (0 knot).

Case no.	$V_s$ [knots]	Wavelength ( $\lambda/L$ )	Wave height (H) [m]	Wave steepness (H/ $\lambda$ )	$f_e$ [Hz] (model)	$T_e$ [sec.] (model)
C71	12	0.75	4.00	1/60	0.9515	1.0510
C72		1.00	5.33		0.7973	1.2542
C73		1.20	6.40		0.7141	1.4004
C73		1.40	7.47		0.6513	1.5355
C81	0	0.75	4.00	1/60	0.7214	1.3862
C82		1.00	5.33		0.6248	1.6006
C83		1.20	6.40		0.5703	1.7534
C84		1.40	7.47		0.5280	1.8939

Heave and pitch responses calculated by the CFD method are compared with the results of the 3-D potential flow method for three ship speeds as shown in Fig. 9. It can be observed in Fig. 9 that 3-D potential flow method heave responses over-estimated the CFD results around the resonant period. This can be explained by the steady and unsteady flow interaction effects on advancing ships. Kim and Shin (2007) showed that in heave and pitch responses the NK approach overestimates the heave and pitch responses compared to the experimental results, whereas they showed that NK approach provides more accurate added resistance estimations of blunt ships compared to the DB method. As it was mentioned before, in the present study, the 3-D linear potential flow method is applied to predict the ship motions and the added resistance using the NK linearization scheme and near-field method in regular waves. It can be observed that at 12 knots and 15.5 knots the heave and pitch response curves show the same patterns. This can be explained by the AFS method because the BVP is solved at zero speed and forward speed corrections are applied to the forward speed cases. It is expected that at higher forward speed cases the order of error will be higher than for the low forward speeds. In zero speed simulations, heave and pitch response patterns are different from the forward speed cases as expected.

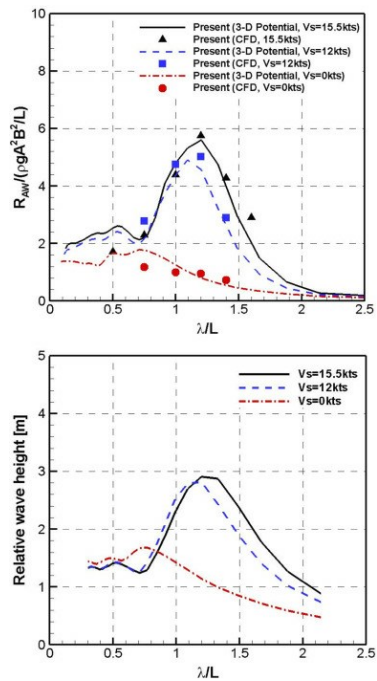


[Download : Download high-res image \(447KB\)](#)

[Download : Download full-size image](#)

Fig. 9. Comparison of heave and pitch responses at different ship speeds ( $V = 0, 12, 15.5$  knots).

The results for the mean added resistance in regular waves are also compared as shown in Fig. 10. The mean added resistance estimated by the 3-D potential and CFD methods show good agreement and it is demonstrated that the added resistance and ship motions can be predicted reliably by using the current numerical approaches. Blok (1993) observed that in head seas the added resistance is increasing with the increase in the ship speed, while the peaks of the added resistance curves shift towards the longer wave periods. In the current study, as it is shown in Fig. 10, Blok's observations are verified for the KVLCC2 and it is observed that the added resistance is augmented with the increase in the ship speed around the resonance period ( $1.0 < \lambda/L < 1.4$ ). However, in short waves the ship speed has minimal effect on the added resistance because in short waves the added resistance is mainly affected by the governing diffraction forces near the bow. Another important phenomenon revealed in Fig. 10 is the close relationship between the added resistance and the relative wave height at Station 18 (130 m forward of midship) where it is observed that the relative motion is the main cause of the added resistance.



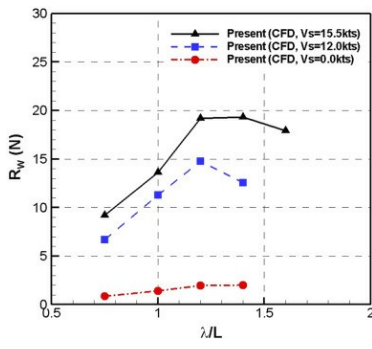
[Download : Download high-res image \(464KB\)](#)

[Download : Download full-size image](#)

Fig. 10. Comparison of added resistance and relative wave height at station 18 at different ship speeds ( $V = 0, 12, 15.5$  knots).

Zeroth order harmonic terms of the total resistance force are also compared using the CFD method for the stationary condition, ship operating and design speeds as shown in Fig. 11. Total resistance in waves increases with increasing ship speed as expected. This is due to the increase in the calm water resistance and the augmented ship motions, hence the increase in added resistance of the ship.



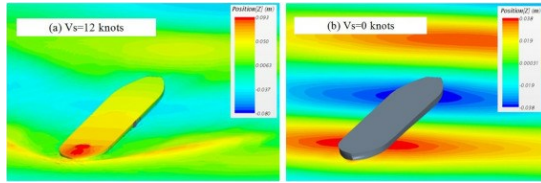


Download : [Download high-res image \(175KB\)](#)

Download : [Download full-size image](#)

Fig. 11. Zeroth order term of harmonic total resistance force in waves with ship speeds (model scale).

For the added resistance resonant case at  $\lambda/L = 1.2$  when the ship is at operational speed and stationary, snapshots of the wave elevation and the vessel motions are illustrated in Fig. 12 at the time instant of  $t/T_e = 0.5$ , when the highest value in added resistance is observed. Green water on deck is observed clearly at the operational speed as shown in Fig. 12(a) where the position (Z) refers to the free surface elevation, while the relative wave elevation around the bow and stern at  $V_s = 0$  knots are clearly observed as presented in Fig. 12(b).

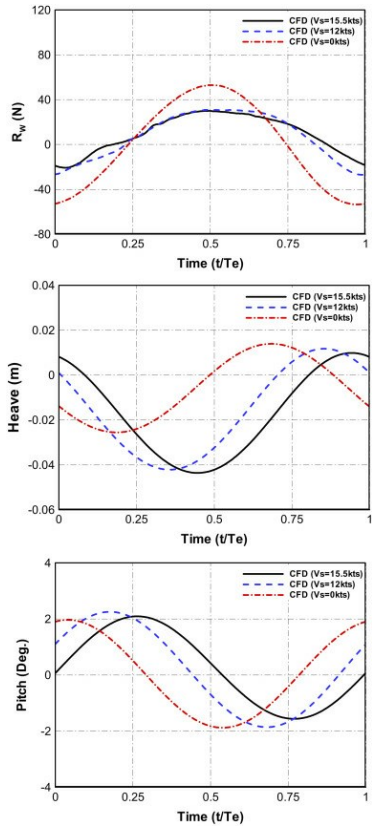


Download : [Download high-res image \(339KB\)](#)

Download : [Download full-size image](#)

Fig. 12. Free surface elevation at the highest added resistance instant ( $t/T_e = 0.5$ ,  $\lambda/L = 1.2$ ).

Time histories of the total resistance and the ship vertical motions at the encounter period are compared for the three ship speeds as shown in Fig. 13. It is observed that in the time domain method the oscillation amplitudes of the total resistance force in waves at the stationary condition are higher than at other speeds even though for the stationary condition the mean total resistance in waves is much lower than the other ship speeds, as shown in Fig. 11. It is shown in Fig. 12 that unlike the forward speed simulations, at the stationary condition there is no green water incidence observed. It should be noted that vessels in stationary condition should be carefully operated in heavy weather conditions because the transient drift forces at zero speed may be larger than the transient drift forces of a vessel advancing in waves. It is also noted that there are serious concerns regarding the ship manoeuvrability at low speed in restricted areas in adverse weather conditions (Shigunov and Papanikolaou, 2015).



Download : [Download high-res image \(598KB\)](#)

Download : [Download full-size image](#)

Fig. 13. Total resistance, heave and pitch responses over one period of encounter ( $\lambda/L = 1.2$ , model scale).

#### 4.4. Added resistance and ship motions with varying wave steepness

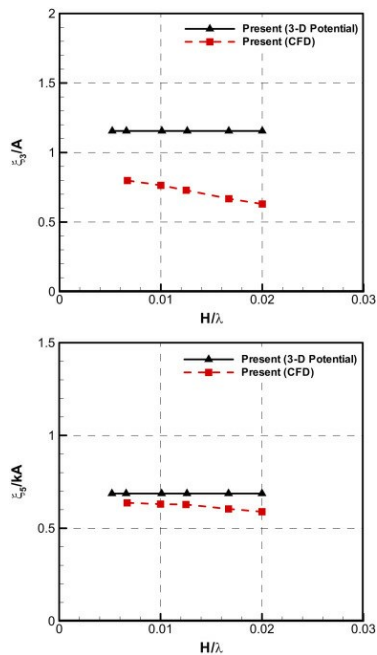
The relationship between the added resistance and the ship vertical motions for the wave steepness ( $H/\lambda$ ) are investigated for a single wavelength ( $\lambda/L = 1.2$ ) at the design speed ( $V_s = 15.5$  knots) as summarised in Table 5.



Table 5. Test cases for wave steepness at  $V_s = 15.5$  knots.

Case no.	Wavelength ( $\lambda/L$ )	Wave steepness ( $H/\lambda$ )	Wave height ( $H$ ) [m]	$f_e$ [Hz] (model)	$T_e$ [sec.] (model)
C20	1.2	1/150	2.56	1.3293	0.7523
C30		1/100	3.84	1.0186	0.9818
C40		1/80	4.80	0.8476	1.1798
C10		1/60	6.40	0.7560	1.3227
C50		1/50	7.68	0.6332	1.5793

Fig. 14 presents the results of the first order harmonic amplitudes of the non-dimensional vertical ship motions with varying wave steepness obtained from the CFD analysis, and the comparison of these results with those obtained from the 3-D panel code. These comparisons indicate that the vertical motions calculated using CFD, especially the heave motions, decrease non-linearly with the increase in wave steepness ( $H/\lambda$ ).

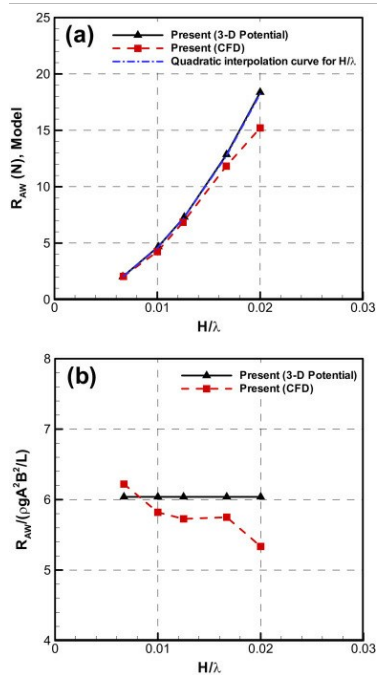


[Download : Download high-res image \(258KB\)](#)

[Download : Download full-size image](#)

Fig. 14. 1st order harmonic terms of non-dimensional heave and pitch responses for different wave steepness ( $V_s = 15.5$  knots,  $\lambda/L = 1.2$ ).

The results of the added resistance calculated using CFD are compared with the 3-D potential results which are almost identical to the quadratic interpolation curve as shown in Fig. 15(a), which indicates that the increase in the added resistance is related quadratically to the increase in the wave height. Additionally added resistance coefficient is presented in Fig. 15(b) which shows that results obtained from CFD decrease non-linearly with the increase in wave steepness. Therefore wave height has a crucial importance in the estimation of the added resistance due to its influence on the relative wave elevation. For this reason, during the design stage for a new vessel, realistic weather conditions should play a vital role in the calculation of accurate added resistance.



[Download : Download high-res image \(337KB\)](#)

[Download : Download full-size image](#)

Fig. 15. (a) Added resistance with varying wave steepness at model scale (b) added resistance coefficient with varying wave steepness ( $V_s = 15.5$  knots,  $\lambda/L = 1.2$ ).

## 5. Conclusions

The added resistance and the vertical ship motions (heave and pitch) in regular head waves were simulated using the unsteady RANS and the 3-D potential flow methods for a broad range of wave conditions at three ship speeds which are the design speed ( $V_s = 15.5$  knots), operating speed ( $V_s = 12$  knots) and zero speed ( $V_s = 0$  knots).

The time histories of the total resistance and the ship motions in waves calculated using the CFD method were examined at zero, design and operational speed taking into account the unsteady wave patterns and viscous effects. The relationship between the resistance force and the ship motions were investigated with varying wave steepness.

Firstly the optimal mesh system was established from the grid convergence tests for the CFD simulations. The resistance and the ship motions in waves in the time domain by CFD oscillate periodically at the encounter period for each test case as was expected.

Secondly the results of the added resistance and the ship motions in regular waves using the CFD and 3-D potential methods were compared with the results of experiments at design speed and were found to be in reasonable agreement except around the heave resonance period ( $1.0 < \lambda/L < 1.4$ ) where both methods underestimate the added resistance. The heave motions were overestimated by 3-D potential method around the resonance period ( $1.0 < \lambda/L < 1.4$ ) and in long waves ( $\lambda/L > 2$ ) due to the AFS formulation. The heave motions were slightly underestimated by the CFD method for the range of wavelengths ( $\lambda/L$ ) from 1 to 1.4 because of the adoption of the non-inertial reference frame. These discrepancies around the resonance period would be investigated in future studies using a developed 3-D potential method and adaptive mesh method in CFD simulations. The wave snapshots and the vessel motions are investigated with the time history data of the resistance force and the vertical motions at the encounter period. For the case C10 ( $V_s = 15.5$  knots,  $\lambda/L = 1.2$ ), the largest added resistance in waves appeared when bow slamming was observed, at the instant when the wave elevation was high around the bow and the ship had the largest immersion even though the pitch amplitude was almost zero.

Thirdly the zeroth order harmonic terms of the total resistance calculated by the CFD method were compared for three ship speeds. The mean total resistance forces were larger for faster ship speeds as expected. However, it was observed that the oscillation magnitude of the total resistance force in the time domain at the stationary speed was larger than at the design and operating speeds.

Fourthly for the resonant test case ( $\lambda/L = 1.2$ ) the wave elevation and the ship motions were examined at the operating and stationary speeds. When the ship had the largest resistance, green water on deck was observed at the operating speed, while the high wave elevations around the bow and stern were seen clearly for the stationary case without water on deck. From the comparison of the time histories of the total resistance and the ship motions at the resonance period, the oscillation magnitudes of the resistance force at  $V_s = 0$  knots were higher than other ship speeds although the zeroth order term of the resistance force was much lower than other ship speeds. Therefore it should be noted that vessels in stationary condition should be carefully operated in heavy weather conditions because the transient drift forces at zero speed may be larger than the transient drift forces of a vessel advancing in waves. It is also likely that the resistance in waves for the ship at zero speed is affected by relative wave elevation around bow and stern since the relative wave height governs the added resistance calculations.

Finally, the relationship between the added resistance and the vertical ship motions were investigated with varying wave steepness at the design speed around the resonance period. It was observed that the vertical ship motion amplitudes obtained from the CFD analysis, especially heave motion, increased non-linearly with the increasing wave steepness ( $H/\lambda$ ) and the added resistance is approximately proportional to the square of the wave height.


## Acknowledgements

The authors are grateful to the Engineering and Physical Research Council (EPSRC) for funding the research reported in this paper through the project: "Shipping in Changing Climate". (EPSRC grant no. [EP/K039253/1](#)).

The results given in the paper were obtained using the EPSRC funded ARCHIE-WeSt High-Performance Computer ([www.archie-west.ac.uk](#)). EPSRC grant no. [EP/K000586/1](#).

Special issue articles   Recommended articles   Citing articles (39)

## References

- Arribas, 2007 F. Arribas  
**Some methods to obtain the added resistance of a ship advancing in waves**  
Ocean Eng., 34 (7) (2007), pp. 946-955  
[View Record in Scopus](#)   [Google Scholar](#)
- Blok, 1993 J.J. Blok  
**The Resistance Increase of a Ship in Waves**  
Delft University of Technology, TU Delft (1993)  
[Google Scholar](#)
- Böckmann et al., 2014 Böckmann, A., Pákozdi, C., Kristiansen, T., Jang, H., Kim, J., 2014. An experimental and computational development of a benchmark solution for the validation of numerical wave tanks. In: Proceedings of the 33rd International Conference on Ocean, Offshore and Arctic Engineering. ASME.  
[Google Scholar](#)
- Deng et al., 2010 Deng, G., Leroyer, A., Guilmineau, E., Queutey, P., Visonneau, M., Wackers, J., 2010. Verification and validation for unsteady computation. In: Proceedings of the Gothenburg 2010: A Workshop on CFD in Ship Hydrodynamics. Gothenburg, Sweden.  
[Google Scholar](#)
- El Mactar et al., 2010 El Mactar, B., Kaufmann, J., Ley, J., Oberhagemann, J., Shigunov, V., Zorn, T., 2010. Prediction of ship resistance and ship motions using RANSE. In: Proceedings of the Workshop on Numerical Ship Hydrodynamics. Gothenburg, p. 1.  
[Google Scholar](#)
- Faltinsen et al., 1980 Faltinsen, O.M., Minsaas, K.J., Liapis, N., Skjördal, S.O., 1980. Prediction of resistance and propulsion of a ship in a seaway. In: Proceedings of the 13th Symposium on Naval Hydrodynamics, Tokyo, pp. 505–529.  
[Google Scholar](#)
- Gerritsma and Beukelman, 1972 J. Gerritsma, W. Beukelman  
**Analysis of the resistance increase in waves of a fast cargo ship**  
Int. Shipbuild. Prog., 19 (217) (1972)  
[Google Scholar](#)
- Gothenburg, 2010 Gothenburg, 2010. A Workshop on Numerical Ship Hydrodynamics, Denmark.  
[Google Scholar](#)
- Guo et al., 2012 B. Guo, S. Steen, G. Deng  
**Seakeeping prediction of KVLCC2 in head waves with RANS**  
Appl. Ocean Res., 35 (2012), pp. 56-67  
[Article](#)    [Download PDF](#)   [View Record in Scopus](#)   [Google Scholar](#)
- Havelock, 1937 T.H. Havelock  
**The resistance of a ship among waves**  
Proc. R. Soc. Lond. Ser. A Math. Phys. Sci. (1937), pp. 299-308  
[View Record in Scopus](#)   [Google Scholar](#)
- Hizir, 2015 O.G. Hizir  
**Three Dimensional Time Domain Simulation of Ship Motions and Loads in Large Amplitude Waves**  
Naval Architecture, Ocean and Marine Engineering, University of Strathclyde, Glasgow (2015)  
[Google Scholar](#)
- IMO, 2012 IMO  
**Interim Guidelines for the Calculation of the Coefficient  $f_w$  for Decrease in Ship Speed in a Representative Sea Condition for Trial Use**  
International Maritime Organisation (IMO), London (2012)  
[Google Scholar](#)

IMO, 2013 IMO

**Interim Guidelines for Determining Minimum Propulsion Power to Maintain the Manoeuvrability in Adverse Conditions**

International Maritime Organisation (IMO), London (2013)

[Google Scholar](#)

ITTC, 2014 ITTC, 2014. The Specialist Committee on Seakeeping-final Report and Recommendations to the 27th ITTC, International Towing Tank Conference, Copenhagen.

[Google Scholar](#)

Joncquez, 2009 S.A. Joncquez

**Second-Order Forces and Moments Acting on Ships in Waves**

Technical University of Denmark, Copenhagen, Denmark (2009)

[Google Scholar](#)

Joosen, 1966 Joosen, W.P.A., 1966. Added resistance of ships in waves. In: Proceedings of the 6th Symposium on Naval Hydrodynamics. National Academy Press, Washington D.C.

[Google Scholar](#)

Kim and Shin, 2007 B. Kim, Y.S. Shin

**Steady flow approximations in three-dimensional ship motion calculation**

J. Ship Res., 51 (3) (2007), pp. 229-249

[CrossRef](#) [View Record in Scopus](#) [Google Scholar](#)

Kim et al., 2014 H.T. Kim, J.J. Kim, N.Y. Choi, G.H. Lee

**A study on the operating trim, shallow water and wave effect**

SNAK (2014), pp. 631-637

[View Record in Scopus](#) [Google Scholar](#)

Kim et al., 2007 K.H. Kim, Y. Kim, Y. Kim

**WISH JIP Project Report and Manual**

Marine Hydrodynamic Laboratory, Seoul National University (2007)

[Google Scholar](#)

Kim et al., 2012 K.H. Kim, M.G. Seo, Y.H. Kim

**Numerical analysis on added resistance of ships**

Int. J. Offshore Polar Eng., 22 (01) (2012), pp. 21-29

[View Record in Scopus](#) [Google Scholar](#)

Kim et al., 2016 Kim, M., Hizir, O., Turan, O., Day, S., Incecik, A., 2016. A study on ship speed loss due to added resistance in a seaway. In: Proceedings of the 26th International Ocean and Polar Engineering Conference. Int. Soc. Offshore Polar Eng. Rhodes, Greece, pp. 527–534.

[Google Scholar](#)

Kim and Park, 2015 M. Kim, D.W. Park

**A study on the green ship design for ultra large container ship**

J. Korean Soc. Mar. Environ. Saf., 21 (5) (2015), pp. 558-570

[CrossRef](#) [View Record in Scopus](#) [Google Scholar](#)

Kim et al., 2015 Kim, Y.C., Kim, K.S., Kim, J., Kim, Y.S., Van, S.H., Jang, Y.H., 2015. Calculation of added resistance in waves for KVLCC2 and its modified hull form using RANS-based method. In: Proceedings of the 25th International Offshore and Polar Engineering Conference. Int. Soc. Offshore Polar Eng. Hawaii, USA, pp. 924–930.

[Google Scholar](#)

Kwon, 2008 Y.J. Kwon

**Speed loss due to added resistance in wind and waves**

Nav. Archit. (2008), pp. 14-16

[View Record in Scopus](#) [Google Scholar](#)

Larsson et al., 2010 Larsson, L., Stern, F., Visonneau, M., 2010. Proceedings Gothenburg 2010. In: Technology, C.U.o. (Ed.) A Workshop on Numerical Ship Hydrodynamics, Gothenburg, Sweden.

[Google Scholar](#)

Lee and Sclavounos, 1989 C.H. Lee, P.D. Sclavounos

**Removing the irregular frequencies from integral equations in wave-body interactions**

J. Fluid Mech., 207 (1989), pp. 393-418

[View Record in Scopus](#) [Google Scholar](#)

Lee et al., 2013 Lee, J.H., Seo, M.G., Park, D.M., Yang, K.K., Kim, K.H., Kim, Y., 2013. Study on the effects of hull form on added resistance. In: Proceedings of the 12th International Symposium on Practical Design of Ships and Other Floating Structures. Changwon, Korea, pp. 329–337.

[Google Scholar](#)

Liu et al., 2011 S. Liu, A. Papanikolaou, G. Zaraphonitis

**Prediction of added resistance of ships in waves**

Ocean Eng., 38 (4) (2011), pp. 641-650

[Article](#)  [Download PDF](#) [View Record in Scopus](#) [Google Scholar](#)

Mauro, 1960 H. Mauro

**The drift of a body floating on waves**

J. Ship Res., 4 (1960), pp. 1-5

[Google Scholar](#)

Newman, 1967 J.N. Newman

**The drift force and moment on ships in waves**

J. Ship Res., 11 (1) (1967), pp. 51-60

[CrossRef](#) [View Record in Scopus](#) [Google Scholar](#)

Park et al., 2014 D.M. Park, M.G. Seo, J. Lee, K.Y. Yang, Y. Kim

**Systematic experimental and numerical analyses on added resistance in waves**

J. Soc. Nav. Archit. Korea, 51 (6) (2014), pp. 459-479

[View Record in Scopus](#) [Google Scholar](#)

Prpić-Oršić and Faltinsen, 2012 J. Prpić-Oršić, O.M. Faltinsen

**Estimation of ship speed loss and associated CO2 emissions in a seaway**

Ocean Eng., 44 (2012), pp. 1-10

[Article](#)  [Download PDF](#) [View Record in Scopus](#) [Google Scholar](#)

Sadat-Hosseini et al., 2010 Sadat-Hosseini, H., Carrica, P., Kim, H., Toda, Y., Stern, F., 2010. URANS simulation and validation of added resistance and motions of the KVLCC2 crude carrier with fixed and free surge conditions. Gothenburg 2010: A Workshop on CFD in Ship Hydrodynamics.

[Google Scholar](#)

Sadat-Hosseini et al., 2013 H. Sadat-Hosseini, P. Wu, P. Carrica, H. Kim, Y. Toda, F. Stern

**CFD verification and validation of added resistance and motions of KVLCC2 with fixed and free surge in short and long head waves**

Ocean Eng., 59 (2013), pp. 240-273

[Article](#)  [Download PDF](#) [View Record in Scopus](#) [Google Scholar](#)

[Salvesen et al., 1970](#) N. Salvesen, E.O. Tuck, O.M. Faltinsen

**Ship motions and sea loads**

SNAME, 104 (1970), pp. 119-137

[View Record in Scopus](#) [Google Scholar](#)

[Seo et al., 2014](#) M.G. Seo, K.K. Yang, D.M. Park, Y. Kim

**Numerical analysis of added resistance on ships in short waves**

Ocean Eng., 87 (2014), pp. 97-110

[Article](#)  [Download PDF](#) [View Record in Scopus](#) [Google Scholar](#)

[Shen and Wan, 2013](#) Z. Shen, D. Wan

**RANS computations of added resistance and motions of a ship in head waves**

Int. J. Offshore Polar Eng., 23 (04) (2013), pp. 264-271

[View Record in Scopus](#) [Google Scholar](#)

[Shigunov and Papanikolaou, 2015](#) V. Shigunov, A. Papanikolaou

**Criteria for minimum powering and maneuverability in adverse weather conditions**

Ship Technol. Res., 62 (3) (2015), pp. 140-147

[CrossRef](#) [View Record in Scopus](#) [Google Scholar](#)

[SHOPERA, 2016](#) SHOPERA, 2016. Energy Efficient Safe Ship Operation EU FP-7 Project.

[Google Scholar](#)

[SIMMAN, 2014](#) SIMMAN, 2014. Workshop on Verification and Validation of Ship Manoeuvring Simulation Methods. Denmark.

[Google Scholar](#)

[Stern et al., 2006](#) F. Stern, R. Wilson, J. Shao

**Quantitative V&V of CFD simulations and certification of CFD codes**

Int. J. Numer. Methods Fluids, 50 (11) (2006), pp. 1335-1355

[CrossRef](#) [View Record in Scopus](#) [Google Scholar](#)

[Tezdogan et al., 2015](#) T. Tezdogan, Y.K. Demirel, P. Kellett, M. Khorasanchi, A. Incecik, O. Turan

**Full-scale unsteady RANS CFD simulations of ship behaviour and performance in head seas due to slow steaming**

Ocean Eng., 97 (2015), pp. 186-206

[Article](#)  [Download PDF](#) [View Record in Scopus](#) [Google Scholar](#)

[Van't Veer, 2009](#) Van't Veer, A.P., 2009. PRECAL v6.5 Theory Manual.

[Google Scholar](#)

[View Abstract](#)



[About ScienceDirect](#)  
[Remote access](#)  
[Shopping cart](#)  
[Advertise](#)  
[Contact and support](#)  
[Terms and conditions](#)  
[Privacy policy](#)

We use cookies to help provide and enhance our service and tailor content and ads. By continuing you agree to the [use of cookies](#).  
Copyright © 2021 Elsevier B.V. or its licensors or contributors. ScienceDirect® is a registered trademark of Elsevier B.V.  
ScienceDirect® is a registered trademark of Elsevier B.V.



FEEDBACK A small icon of a speech bubble with a question mark inside, used for feedback.